Elucidating the Origin of Diastereoselectivity in a Self-Replicating System: Selfishness versus Altruism
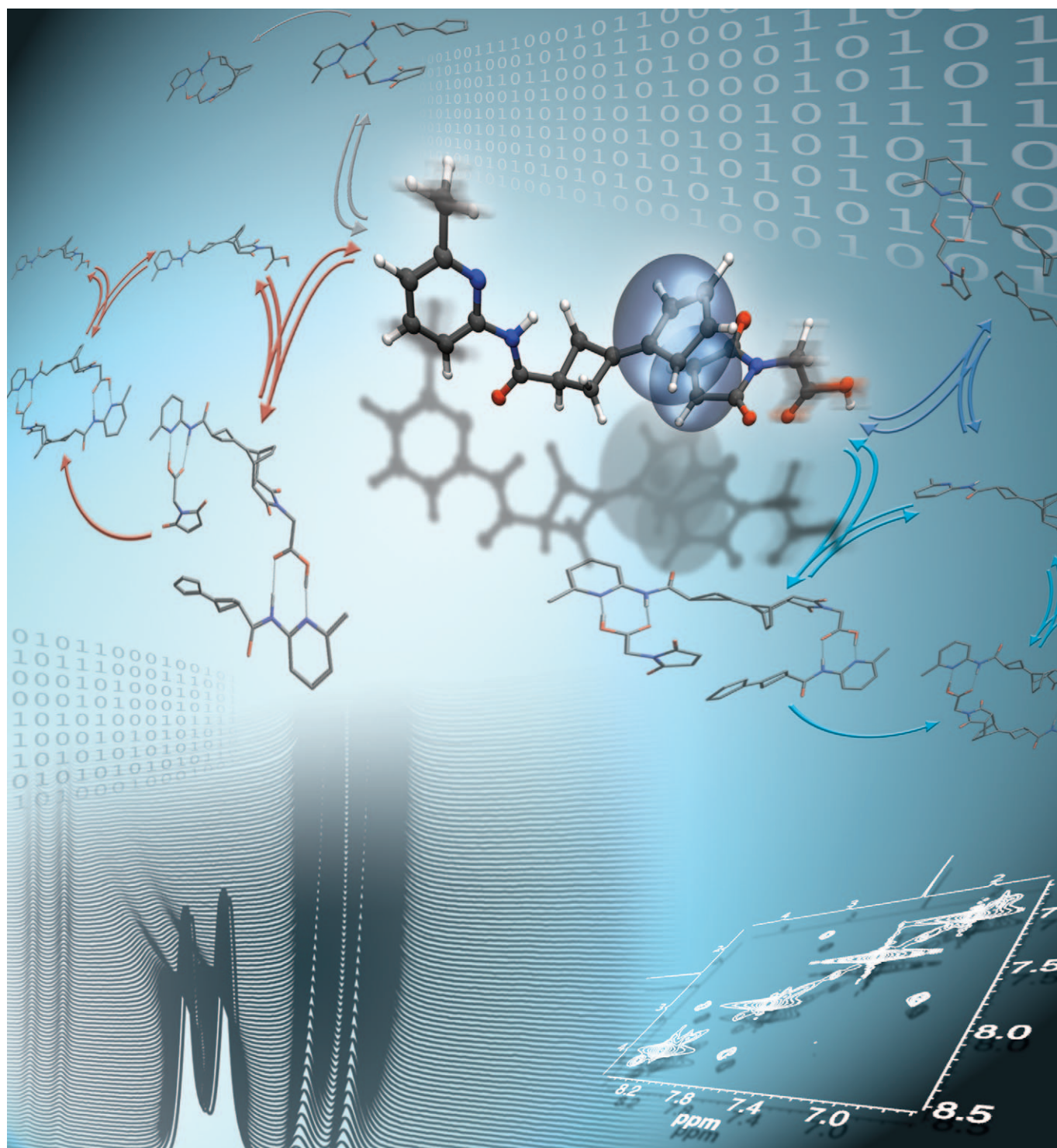
Arne Dieckmann,*[a] **Sabrina Beniken,**[b] **Christian D. Lorenz,**[c] **Nikos L. Doltsinis,**[b] **and Günter von Kiedrowski**[a]

Abstract: We have investigated a diastereoselective self-replicating system based on a cycloaddition of a fulvene derivative and a maleimide using a two-pronged approach of combining NMR spectroscopy with computational modelling. Two diastereomers are formed with identical rates in the absence of replication. When replication is enabled, one diastereomer takes over the resources as a "selfish" auto-catalyst, while exploiting the competitor as a weak "altruist", resulting in a diastereoselectivity of 16:1. We applied 1D and 2D NMR spectroscopic techniques supported by ab initio chemical shifts as well as ab initio molecular dynamics simulations to study the structure and dynamics of the underlying network. This powerful combination allowed us to decipher the energetic and structural rationale behind the observed behaviour, while static computational methods currently used in the field did not.

Keywords: kinetics · molecular dynamics · NMR spectroscopy · self-replication · supramolecular chemistry

Introduction

The emerging field of systems chemistry[1–3] set itself an ambitious goal, namely, the design of pre-specified dynamic behaviour of complex chemical reaction systems. The kind of phenomena this new research area deals with spans from chiral symmetry breaking[4–19] and spatio-temporal pattern formation[20,21] to self–replication.[22–68] However, the ability to understand always precedes the ability to design. Establishing the relationship between molecular structure and thermodynamic or kinetic parameters determining the observed macroscopic behaviour of a system is often a challenge, either due to a large number of interdependent parameters or experimental obstacles hampering the application of certain analytical methods. Clearly, there is a growing necessity to widen the scope of analytical techniques and to include theoretical approaches as well because they can provide information that is inaccessible experimentally. The challenge for the near future will be to find a convergent route that is characterised by an interplay of experiment and theory. Herein, we describe such an interplay that has resulted in a detailed understanding and unravelling of a diastereoselective self-replicating system. The replicator utilises a fulvene-based Diels–Alder reaction in which two diastereomers are formed with identical rates in the absence of catalysis. When replication is enabled, a network emerges in which one diastereomer takes over the resources as a "selfish" autocatalyst, while exploiting the competitor as a weak "altruist", leading to a diastereoselectivity of 16:1. We show that an interplay of ab initio molecular dynamics (AIMD) as developed by Car and Parrinello[69] with NMR kinetics supported by ab initio chemical shifts and 2D NMR spectroscopic methods allow us to rationalise the observed behaviour, while static computational methods currently used in the field are not able to qualitatively reproduce the experimental data. The limited success of theoretical efforts so far may be due to the fact that important entropic effects have not been considered[1,47–49,52] and we anticipate new insights from applying our dynamic approach to similar systems. It brings us a step closer to a goal that has been seen as paramount for systems chemistry: The ability to design and synthesise dynamic signatures not usually found in chemical systems close to equilibrium but in nonequilibrium systems, including biological ones.

In a self-replicating system, autocatalysis is coupled to a transfer of chemical information such as constitution, configuration or long-lived conformation.[22] A minimal scheme of a self-replicating system is depicted in Figure 1. Let us assume two precursors, A and B, are able to react to form C in a bimolecular reaction. Once enough C has been formed it is able to reversibly preorganise precursors A and B—for example, by hydrogen bonding—in a termolecular complex [A·B·C]. Within [A·B·C], a pseudo-unimolecular ligation reaction takes place leading to template duplex C_2. In other

[a] Dr. A. Dieckmann, Prof. Dr. G. von Kiedrowski
Lehrstuhl für Organische Chemie I
Bioorganische Chemie
Ruhr-Universität Bochum
44780 Bochum (Germany)
Fax: (+49)234-3214355
E-mail: arne.dieckmann@rub.de

[b] S. Beniken, Dr. N. L. Doltsinis
Department of Physics
King's College London
WC2R 2LS, London (United Kingdom)

[c] Dr. C. D. Lorenz
Department of Engineering
King's College London
WC2R 2LS, London (United Kingdom)

Supporting information (including synthetic schemes, procedures and characterisation data for all compounds) for this article is available on the WWW under http://dx.doi.org/10.1002/chem.201002325.
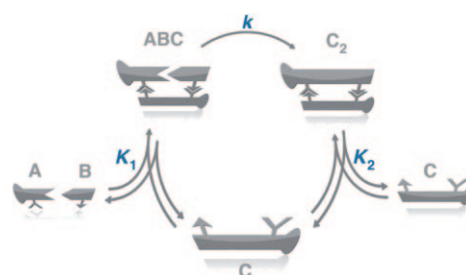
Figure 1. A model of a minimal self-replicating system.

words, the entropy of activation for the reaction is reduced by templating, resulting in an acceleration of reaction rate. After dissociation of C_2, each template may enter another replication cycle. In principle, the number of templates doubles after every cycle resulting in exponential growth. In real systems exponential growth is difficult to achieve, since the type of growth depends on the relative stabilities of [A·B·C] and C_2. Exponential growth can only occur if [A·B·C] is more stable than C_2, which is difficult to accomplish due to intrinsic positive cooperative chelate effects stabilising C_2. Chelate cooperativity might be counterbalanced if ligation is accompanied by a significant change in molecular geometry, leading to unfavourable interactions between both templates.

Our chemical implementation is not based on naturally occuring structures, but on artificial molecules. Small organic replicators offer particular advantages concerning the derivation of structure–reactivity relationships: On the one hand, they are large enough to exhibit autocatalysis coupled to information transfer. On the other hand, they are small enough to be treatable by ab initio electronic structure methods. The general structure of our system is depicted in Scheme 1. Molecules A and B can undergo a Diels–Alder reaction to form four diastereomers: Two *endo* and two *exo* products differing in the relative orientation of the amidopyridine moiety with respect to the bridge. A two-letter code is introduced here to facilitate the nomenclature of diastereomers. The first letter refers to *endo* (N) or *exo* (X) Diels–Alder stereochemistry, the second indicates if substitution of the four-membered ring by the amidopyridine moiety occurs on the same side as the bridge (N) or on the opposite side (X). Only the linear products NN and NX are able to act as a template by preorganising A and B in a termolecular complex. We decided to utilise a fulvene Diels–Alder reaction to construct our replicator for two reasons: First, fulvene chemistry allows a facile variation of the diene part. Second, in contrast to a previously described system,[1] we aimed to avoid enantiomeric reaction products to simplify the kinetic analysis, since they are indistinguishable by NMR spectroscopy. On the other hand, both precursors can be easily modified to introduce another level of complexity, for example, a simple substitution of any hydrogen atom of maleinimide A leads to a chiral product, allowing the study of phenomena such as chiral symmetry breaking.

Results and Discussion

Kinetics of the background reaction: First of all, the reaction between A′ and B was studied to obtain kinetic information about the so-called background reaction in the absence of catalysis, that is, with the carboxylic recognition site blocked on A′ and all products. We obtained concentration–time curves for A′, B and products by time-resolved ^{1}H NMR spectroscopy (600 MHz) at 293 K in CDCl$_3$. The starting concentrations of A′ and B were 15 mM each (Figure 2a).
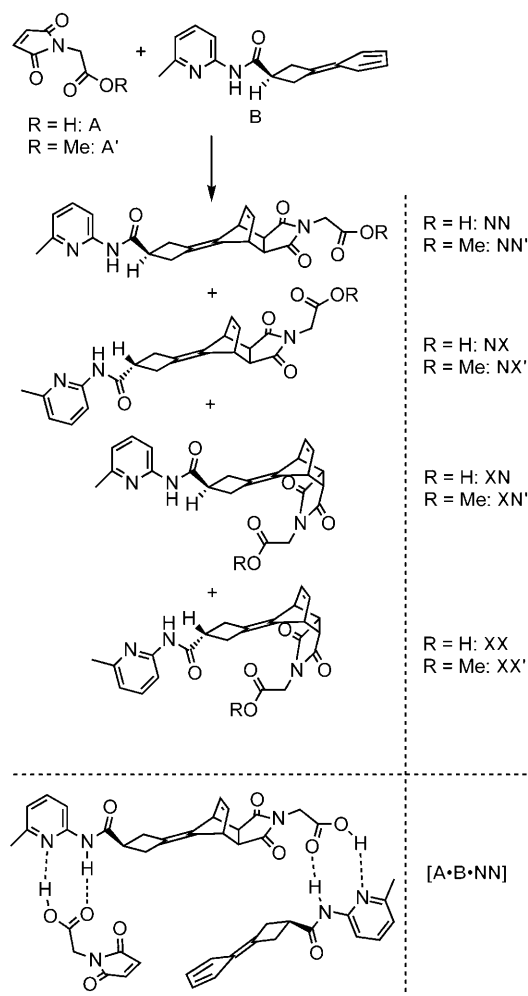
Scheme 1. Molecules A and B can react to form four different diastereomers. Only NN and NX can template their own formation. [A·B·NN] is given as an example.

Surprisingly, the 1D NMR spectra obtained only show one set of product signals, whereas we expected to see at least both *endo* Diels–Alder products NN′ and NX′. HPLC analysis of the product solution indeed revealed two products, the configurations of which could be identified by selective 1D and 2D ROESY NMR spectroscopy as NN′ and NX′. The apparent discrepancy arises from the fact that all 1D NMR signals of both isomers exhibit coincidental isochronicity and thus only produce a single peak. By integration of the HPLC peaks, we determined a slight diastereoselectivity of 2:3 for NN′/NX′ after quantitative conversion. However, this model reaction does not take into account the formation of [A·B] complexes if molecular recognition is allowed, which might have a significant impact on diastereoselectivity. To consider this effect, we set up the reaction of A′ with B again, but this time added two equivalents of unreactive succinimide A* (Figure 2b). A* can bind to B, but is unable to undergo a cycloaddition reaction. We found that the diastereoselectivity of NN′/NX′ was altered to 1:1 in the presence of A*. By inspection of the geometries of [A*·B]
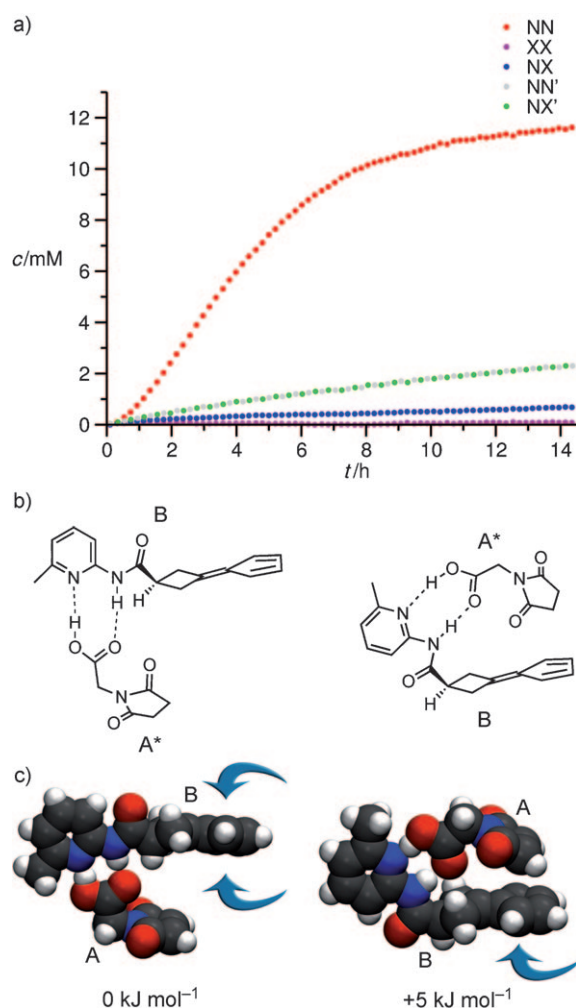
Figure 2. a) Concentration–time curves of the background (green, grey) and autocatalytic (red, blue, violet) reactions. The rate of the background reaction was measured in a separate experiment using A′ and B. b) Succinimde A* was used as a substitute for A to probe the effect of [A*·B] formation on diastereoselectivity of the background reaction. Two possible rotamers are depicted. c) Optimised geometries and relative energies of two rotamers of [A·B]. Arrows indicate possibilities for an attack of B by another molecule A.

and [A·B] (Figure 2 c), it becomes clear that in one of the two possible rotamers one side of B is shielded from an attack of another molecule A. This attack would lead to NX, which explains why the slight selectivity for NX is compensated for. Since the energy difference between the optimised rotamers is just 5 kJ mol^{-1}, both will be populated at 293 K. Moreover, rotation of the amidopyridine moiety, leading to interconversion of both rotamers, occured frequently in AIMD simulations of the Diels–Alder reactions as well as complex dissociations. There is no evidence in the literature that this simple test has been performed previously for other diastereoselective replicators.[44,47,49,50,54,70]

Kinetics of the autocatalyic system: The reaction of A with B was studied under the same conditions as described

above. 1D NMR spectra show the formation of three products, although again most of the signals overlapped. In contrast to the background reaction, there is one clear main product and two side products (see Figure 2 a). The concentration–time curve of the main product has a distinct sigmoidal shape, indicating that autocatalysis might be operative here. To elucidate the structure of all three products, we tried to use HPLC to separate the products, which was not successful due to solubility issues. We observed that product precipitation is kinetically hindered for as long as a few days. Once precipitated, however (e.g., by solvent evaporation), the products could not be dissolved again. In addition, once the solution of a converted reaction was injected into a HPLC column it proved impossible to elute any product. Thus, we decided to run ROESY experiments on the product mixture. This procedure was successful, since it allowed us to decipher the composition of the mixture. We were able to identify three products: NN, NX and XX. Prior to performing ROESY experiments, we had calculated optimised and dynamically averaged structures for all diastereomers and knew interatomic distances for those hydrogen atoms that would allow us to derive the configuration of every isomer. Indeed, we detected the expected NOE effects, which are displayed in Figure 3 b–d. In addition, we realised that one amide NH proton at $\delta = 12.6$ ppm did not undergo chemical exchange, while the other two amide NH signals showed off-diagonal peaks indicating exchange (Figure 3 a). XX is the only diastereomer capable of intramolecular hydrogen bonding and therefore reducing the possibility of exchange, so the signal at $\delta = 12.6$ ppm was attributed to XX. Our analysis revealed that NN is the main product, while NX and XX are present at a much lower concentrations. However, although we were able to identify NX and XX, we were not able to assign each isomer to a set of two non-overlapping 1D NMR signals belonging to the same pyridine proton in different isomers (Figure 3 e). Unfortunately, this proton does not exhibit NOE effects that allow the determination of relative configurations. However, we were still able to identify NN, since it was the main product and had a much larger NMR signal than the other two isomers. In summary, at this point we knew the composition of the product mixture, but were unable to extract time-dependent concentrations for NX and XX.

For direct assignment of the experimental 1D NMR spectra, we calculated thermally averaged ab initio chemical shifts of the [NN·NX] duplex and the XX isomer. We did not calculate shifts for the monomeric NX template because the complex equilibrium after quantitative conversion is strongly shifted towards template duplexes. Since the NX isomer is only present at a low concentration (<1 mM), it is expected to bind quantitatively to the NN isomer rather than populating a homo duplex. The two experimental signals for the pyridine proton displayed in Figure 3 e had chemical shifts of $\delta = 8.38$ and 8.44 ppm, whereas the calculated values for [NN·NX] and XX were $\delta = 8.34$ and 8.45 ppm, respectively. This remarkable agreement allowed us to assign the isomers accordingly and to extract concen-
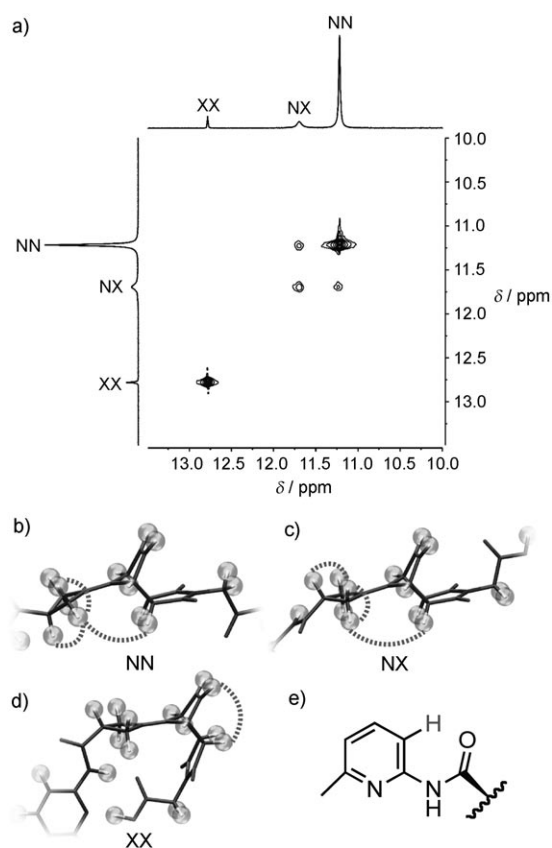
Figure 3. a) Cutout of a ROESY spectrum (see the Experimental Section for details) showing diagonal positive in-phase peaks for NH protons of NN, NX and XX, and positive in-phase cross-peaks originating from chemical exchange between NN and NX. ROE peaks would display negative in-phase absorption. XX is the only product capable of intramolecular hydrogen bonding and thus does not show chemical exchange for its proton. b)–d) NOE effects between protons, allowing the identification of different diastereomers, are marked with dashed lines. The respective cross-peaks were present in all ROESY spectra. e) The 1D NMR signal of this pyridine proton was used to extract time-dependent concentrations for all three isomers.
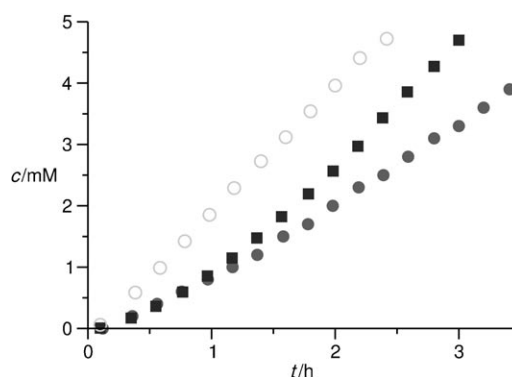

Figure 4. Effect of addition of benzoic acid (2 equiv, ●) and reaction products (10%, ○) on the concentration–time curve of NN in the recognition-mediated system (■).

tration–time curves for both. Our assignment was corroborated by the fact that an inverse assignment did not allow for a good fit of the data to kinetic models that were in accordance with results from our calculations. These will be discussed in detail below.

Concentration–time curves for the recognition-enabled system show a strong NN/NX diastereoselectivity of 16:1. Furthermore, small quantities of XX were observed. To prove that self-replication was operative in the system, we performed two control measurements: First, we added two equivalents of benzoic acid at the beginning of the reaction (Figure 4). Benzoic acid should act as a competitive inhibitor because it will compete with A for amidopyridine recognition sites, but is completely unreactive. This should result in a slower reaction rate after the lag phase, which was clearly visible for NN. The effect on the rate of NX is not detectable due to the low concentration of NX, which causes integration errors of a similar magnitude. Second, we

added a 10% product mixture from another reaction corresponding to an almost pure solution of NN at the start of the reaction; this should increase the reaction rate if NN acts as a template for its own formation by removing the lag phase. Indeed a pronounced increase in initial rate is visible for NN, while it is again impossible to see an effect on the rate of the formation of NX. This will be demonstrated and explained later in this article by kinetic modelling.

Having experimentally proven that NN is capable of self-replication, we investigated whether the same would be true for NX and if both isomers would undergo cross-catalysis, which seems likely based on their similar geometries. The solution to this problem also has to explain the emerging diastereoselectivity and presence of XX or absence of XN.

Molecular dynamics simulations: Since the catalytic properties of each product alone could not be characterised experimentally, mechanistic insights explaining the observed dynamics from another source were required. Instead of relying on single-point calculations for precursors, transition states (TSs) and products, we took into account important entropic effects brought about by the dynamics of the flexible molecular structures, and calculated free-energy profiles rather than purely enthalpic minimum-energy curves. We performed AIMD free-energy calculations of the [4+2] cycloaddition using the recently proposed dynamic distance constraint.[71–73]

The dynamic distance, D, is a versatile constraint especially suited to simulate the rupture or formation of multiple bonds. For the simulation of a Diels–Alder reaction, it corresponds to the root-mean-square (RMS)distance of the new bonds being formed (corresponding to the two distances between the two pairs of carbon atoms, see Figure 5a and b). The reaction is controlled by incrementally decreasing D from 3.6 (precursors) to 1.6 Å (product) and performing an AIMD simulation for every fixed value of D. Free-energy profiles (FEPs) were obtained by thermodynamic integration of the mean constraint force. Minimum-energy paths (MEPs) were obtained by performing geometry optimisations for snapshots from the MD simulations. Errors for
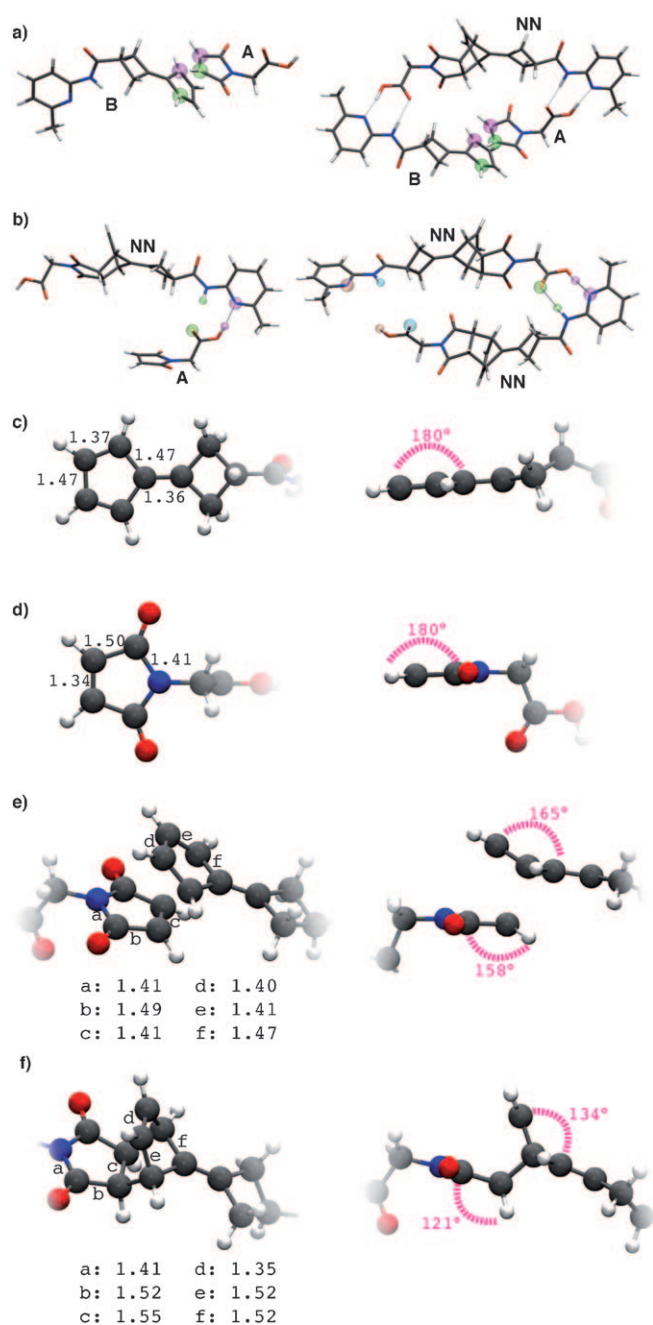
Figure 5. Dynamic distances corresponding to the RMS distance between carbon atoms of the same colour are shown. a) Single distances correspond to the length of the new bonds formed in the course of the Diels–Alder reaction. b) Setup of the dynamic distance for the simulation of complex dissociations. In the case of [A·NN], the constraint contains two distances, in the case of [NN·NN], it contains four. The distances correspond to the length of the respective hydrogen bonds. Bond lengths and angles for c) fulvene, d) maleimide and e) the transition state of a reaction to form NN and f) the NN isomer. These parameters led to the conclusion that an early and synchronous TS was present.

FEPs were estimated by fluctuations of the mean constraint force.

First, we had to ensure that the chosen constraint was able to represent the correct reaction mechanism. For a

[4+2] cycloaddition of a symmetric fulvene and a maleimide, a concerted reaction mechanism with a synchronous TS was expected, which we found using D (Figure 5c–f). To locate a possible biradical mechanism with a lower TS, we performed several single-point calculations and MD simulations using the local spin density approximation, but all attempts converged to the respective closed-shell energies.

Having established the dynamic distance as a suitable reaction coordinate, we simulated all major reaction pathways of the system, that is, templated and non-templated *endo* Diels–Alder reactions to NN and NX and non-templated *exo* Diels–Alder reactions to XN and XX. FEPs and MEPs thus obtained are displayed in Figure 6a–d. First, it is clear that all MEPs exhibit a lower reaction barrier than the FEPs, since MEPs do not factor in entropic contributions. Second, most MEPs possess a substantial ruggedness due to the fact that at each value of D the highly flexible structures B, NN, NX and, in particular, complexes comprised of them possess a large number of local minima. This demonstrates the need to carry out dynamic rather than static studies on these systems because interpreting replicators purely on the basis of 0 K energy barriers obtained from optimised TSs bears considerable uncertainties.[1,47–49,52] This need to use free energies instead of enthalpies has long been recognised in the field of transition-state theory (TST) and has led to the development of variational TST (see, for instance, reference [74] and references therein).

Background reactions to NN and NX have free-energy barriers of 68 and 71 kJ mol^{-1}, respectively (Table 1), which are identical considering the statistical errors in the free-

Table 1. Values of FEP and MEP barriers for all pathways and the product/complexes they give.

Product	FEP [kJ mol^{-1}]	MEP [kJ mol^{-1}]
NN	68 ± 7	63
NX	71 ± 5	61
XN	84 ± 3	58
XX	85 ± 7	68
[NN·NN]	66 ± 7	50
[NN·NX]	72 ± 5	48
[NX·NX]	65 ± 5	53

energy calculations. The slight diastereoselectivity for NX cannot be explained by these energy profiles, since the difference between barriers will be smaller than the error of our calculations. In contrast, a bimolecular reaction to XN, which has not been observed experimentally, features a significantly higher free-energy barrier of 84 kJ mol^{-1} (Figure 6d and Table 1), explaining its absence in the product mixture. Surprisingly, the barrier of the MEP (58 kJ mol^{-1}; Figure 6a) is of comparable height as those for background reactions to NN and NX, suggesting that XN should be formed with a similar rate. This means that MEPs are unable to even qualitatively predict the correct product distribution of the background reactions. The last non-templated pathway is the reaction to XX, which can proceed in a
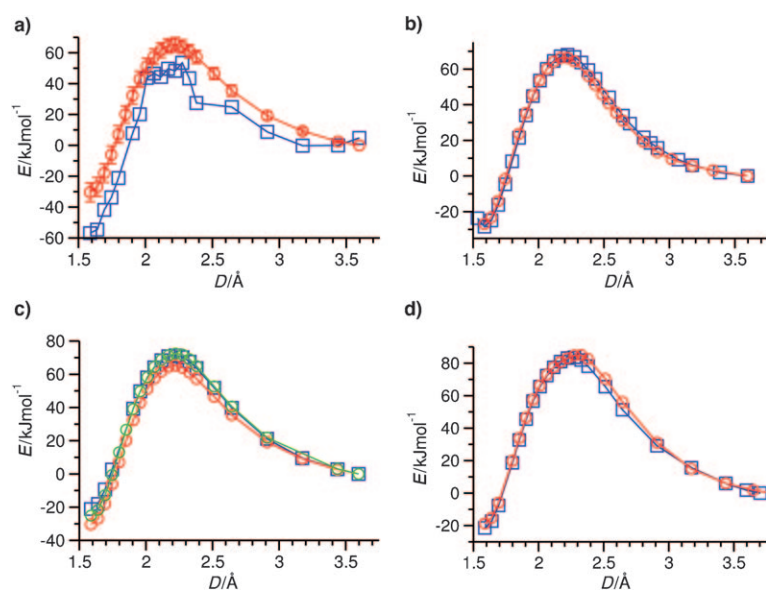
Figure 6. a) A direct comparison of a FEP (○) with estimated errors and MEP (□) for the autocatalytic reaction [A·B·NX]→[NX·NX] is shown as an example. b) FEPs for the bimolecular (□) background reaction to NN and autocatalytic (○) reaction to [NN·NN]. c) FEPs for the bimolecular (□) background reaction to NX, the cross-catalytic (○) reaction to [NN·NX] and the autocatalytic (○) reaction to [NX·NX]. d) FEPs for the bimolecular reaction to XN (□) and the pseudo-unimolecular reaction to XX (○) via an [A·B] complex. Values of FEP and MEP barriers are given in Table 1 for all pathways and labeled by the product/complex they lead to.

plated reactions reveals that the free-energy barriers for autocatalytic reactions are quite similar, whereas the barrier of the cross-catalytic pathway is 6–7 kJ mol^{-1} higher. These barriers are comparable to those of the respective background reactions. On the other hand, a comparison of the MEP barriers (48–53 kJ mol^{-1}) with those of the background reactions (61–63 kJ mol^{-1}) seems to suggest that they are lowered by the presence of a template. Since the kinetic variable is not enthalpy, but free energy, this finding may be rationalised as follows: The catalytic effect of the template is not the result of a change in electronic structure of the TS in its presence, but rather of a change in molecularity of the ligation reaction from second to pseudo-first order without being energetically penalised.

pseudo-unimolecular fashion starting from a suitable conformation of an [A·B] complex (see Figure 7a). This reaction features a free-energy barrier of 85 kJ mol^{-1}, while the minimum energy barrier is much lower (Figure 6). The reason why XX is detected in the recognition-enabled system despite the high barrier is that its formation through a pseudo-intramolecular pathway is kinetically favoured. Such a pathway is not available for XN and thus it is not present either in the background or the recognition-mediated reaction system.

Having reproduced and explained the experimental results for non-templated reactions, we examined auto- and cross-catalytic pathways. In principle, there are four possible templated reactions: [A·B·NN] could catalyse a ligation either to [NN·NN] (autocatalysis) or [NN·NX] (cross-catalysis) and the same holds for [A·B·NX]. Astonishingly, the arrangement of an [A·B·NN] complex that is able to react to form [NX·NN] is impossible due to a geometric mismatch (see Figure 7c). Although both templates look very similar at first sight, NN is more bent than NX, which results in a more acute angle between the recognition sites (see Figure 7b). Which diastereoisomer is produced in a (templated) reaction only depends on the relative orientation of A and B. Since NX is almost linear it is able to arrange the precursors in both orientations, whereas NN is limited to template its own formation. This causes an intrinsic imbalance or asymmetry in the system, namely, a selfish NN template and an altruistic NX template competing for common resources (see Figure 8). The outcome is known from experiments: NN dominates the system, whereas NX is suppressed. A closer look at the free-energy barriers for these three tem-

Figure 7. a) Pseudo-intramolecular reaction to XX. b) NN is more bent than NX, which results in it being unable to cross-catalyse the formation of NX. The angle is measured with respect to the orientation of the exocyclic double bond connected to the four-membered ring. c) Geometries of termolecular complexes. A+B+NN exemplifies the impossible situation of NN acting as a cross-catalyst. [A·B·NX] will react to form [NN·NX], [A·B·NX]* to form [NX·NX].
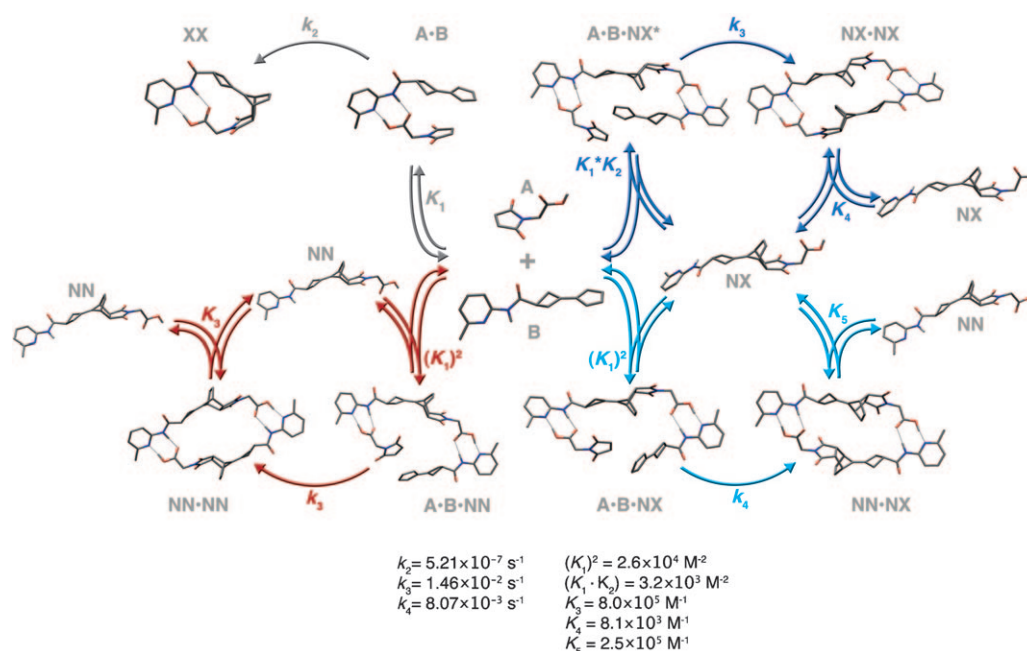
Figure 8. Network of all recognition-mediated pathways of the system with assigned rate and association constants. The pathway catalysed by NN is drawn in red and both pathways catalysed by NX are in blue.

Apart from energetics of ligation reactions, relative complex stabilities are of great importance to understand a self-replicating system, since they determine the type of autocatalyic growth. As mentioned before, replicators often suffer from a high stability of template duplexes, which originates from positive cooperative chelate effects. To get a feeling for the amount of cooperativity operating in our system, we calculated complex dissociation energies of [A·NN] and [NN·NN]. [A·NN] is a good model for all complexes in the system being bound by just one recognition site, while [NN·NN] should exhibit cooperative effects if not destabi-

lised by a change of geometry during ligation. We used the same dynamic distance method as described for the Diels–Alder reaction, but this time the dynamic distance was composed of two ([A·NN]) and four ([NN·NN]) hydrogen bonds, respectively (Figure 5b). Simulations started at $D = 1.66$ Å and D was increased until complete dissociation of the respective hydrogen bonds. The obtained FEPs of dissociation are displayed in Figure 9. Since these simulations are very time consuming, we have only calculated two potentials to date. Both curves level off at intermediate values of D corresponding to the dissociation of the first hydrogen
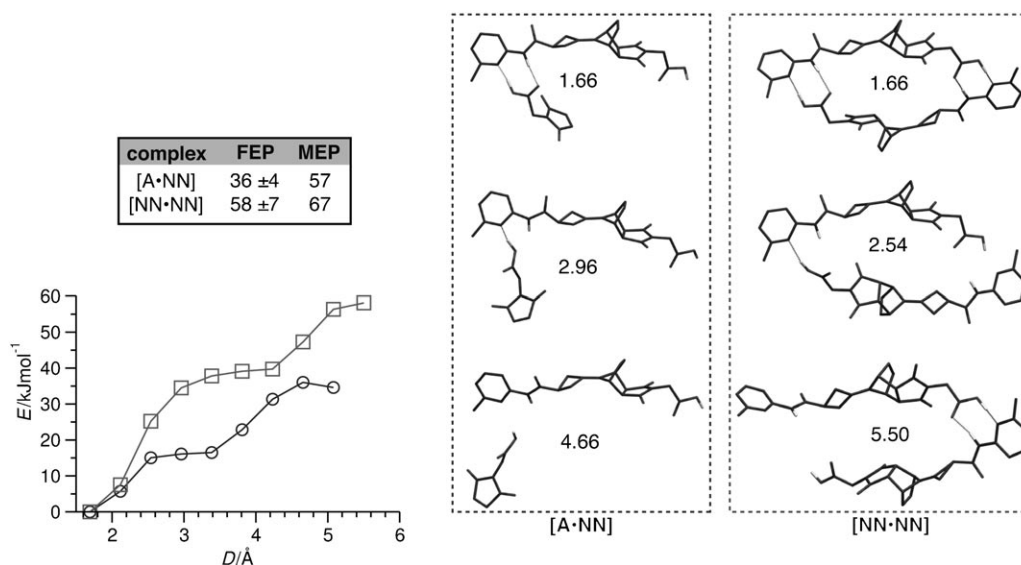

Figure 9. FEPs for the dissociation of one pair of recognition sites in each complex [A·NN] (○) and [NN·NN] (□). Representative geometries of both dissociation processes are displayed for certain values of D. Energies are given in kJ mol^{-1}, values for D in Å.

bond of a recognition site. By further increasing D the second hydrogen bond finally dissociates. It has to be stressed that for [NN·NN] only the dissociation of the first recognition site (i.e., two hydrogen bonds) was calculated, since the simulation follows the path of minimum (free) energy and will keep one recognition site intact until very large values of D are approached. However, cooperative effects are expected to occur only for the dissociation of the first two hydrogen bonds.

A comparison of free-energy changes associated with the dissociation of one recognition site (two hydrogen bonds) in [A·NN] and [NN·NN] clearly shows strong positive cooperative effects in [NN·NN], since its free energy of dissociation is 1.6 times higher than that of [A·NN]. As a consequence, the system should suffer from product inhibition. The change in free energy, ΔG, relates directly to the corresponding equilibrium constant, K, as shown in Equation (1), in which R is the ideal gas constant and T the temperature:

$$\Delta G = -RT\ln K \tag{1}$$

The complete two-step dissociation of all four hydrogen bonds of [NN·NN] can be approximated by the sum of both calculated free-energy changes to be 94 kJ mol^{-1}, since only the first step is cooperative. The relationship shown in Equation (2), in which K_i are association constants, can be easily derived from Equation (1):

$$\frac{\Delta G_{diss}[NN \cdot NN]}{\Delta G_{diss}[A \cdot NN]} = \frac{\ln K_{[NN\cdot NN]}}{\ln K_{[A\cdot NN]}} \tag{2}$$

This equation provides a verifiable test for the results of our simulations and will be revisited later in this article.

Because we have been unable, to date, to calculate free energies of dissocation for more than these two complexes, we needed another method to sort FEPs for templated Diels–Alder reactions. First, we decided to base our ranking on duplexes rather than termolecular complexes because they are more rigid and can be directly detected by NMR spectroscopy. Second, we did not want to rely on single-point energies due to the problems mentioned earlier. Therefore, we calculated average energies from AIMD simulations for all duplexes and used those to sort reaction pathways. As a result, we obtained the energy profile shown in Figure 10. Our simulations predict that [NN·NX] and [NX·NX] are destabilised with respect to [NN·NN]. Interestingly, relative stabilities correlate with the number of inward pointing bridges resulting from the Diels–Alder reaction. It is conceivable by inspection of the duplex geometries that these cause repulsive steric interactions. The energetic distribution of preorganised termolecular complexes is quite different: [A·B·NN] and [A·B·NX] are much more stable than [A·B·NX]*. This finding can be rationalised by the fact that [A·B·NX]* is the only complex in which the inward-pointing bridge of the template and fulvene B have to be brought into close proximity, again resulting in repulsive steric interactions. In summary, auto- and cross-catalytic pathways
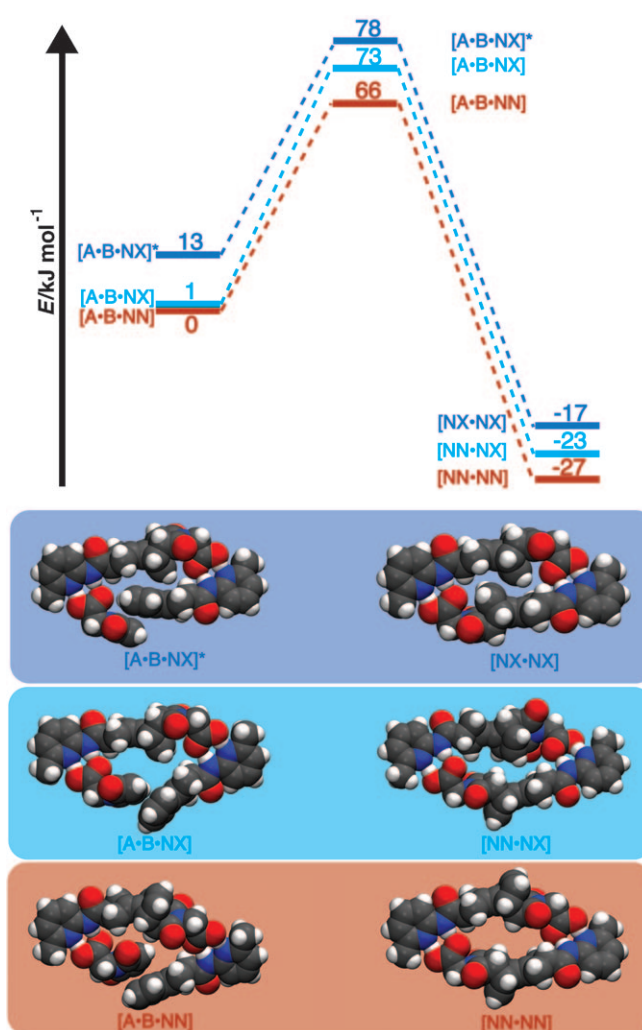
Figure 10. Free-energy profiles for all templated reaction pathways ordered by average energies of duplexes.

leading to the formation of a new molecule, NN, are more favourable than the reproduction of NX; this explains the experimental finding of a 16:1 diastereoselectivity in favour of NN. All recognition-mediated pathways are summarised in Figure 8.

Kinetic modelling: Based on our results from simulations and calculations, we constructed a kinetic model of the system (Figure 11). Complex associations of [A·B·NN] and [A·B·NX] complexes were modelled with the same association constant, whereas [A·B·NX]* was modelled with a separate association constant to account for different relative complex energies. For the same reason, all three duplex equilibria were attributed different association constants. Different rate constants were assigned to auto- and cross-catalytic ligations. The rate constant for uncatalysed reactions to NN and NX was known from separate measurements of the background reaction. Complex associations were assumed to be limited by diffusion and only dissociation was modelled with a variable rate constant. To quantify the rate constants for these processes, a series of classical

$$A + B \xrightarrow{k_1} NN$$

$$A + B \underset{}{\overset{K_1}{\rightleftharpoons}} [A \cdot B]$$

$$A + NN \underset{}{\overset{K_1}{\rightleftharpoons}} [A \cdot NN]$$

$$B + NN \underset{}{\overset{K_1}{\rightleftharpoons}} [B \cdot NN]$$

$$A + B \xrightarrow{k_1} NX$$

$$A + NX \underset{}{\overset{K_1}{\rightleftharpoons}} [A \cdot NX]$$

$$B + NX \underset{}{\overset{K_1}{\rightleftharpoons}} [B \cdot NX]$$

$$AB \xrightarrow{k_2} XX$$

$$[A \cdot NN] + B \underset{}{\overset{K_1}{\rightleftharpoons}} [A \cdot B \cdot NN]$$

$$[B \cdot NN] + A \underset{}{\overset{K_1}{\rightleftharpoons}} [A \cdot B \cdot NN]$$

$$[A \cdot NX] + B \underset{}{\overset{K_1}{\rightleftharpoons}} [A \cdot B \cdot NX]$$

$$[B \cdot NX] + A \underset{}{\overset{K_1}{\rightleftharpoons}} [A \cdot B \cdot NX]$$

$$[A \cdot NX] + B \underset{}{\overset{K_2}{\rightleftharpoons}} [A \cdot B \cdot NX]^*$$

$$[B \cdot NX] + A \underset{}{\overset{K_2}{\rightleftharpoons}} [A \cdot B \cdot NX]^*$$

$$[A \cdot B \cdot NN] \xrightarrow{k_3} NN_2$$

$$[A \cdot B \cdot NX]^* \xrightarrow{k_3} NX_2$$

$$[A \cdot B \cdot NX] \xrightarrow{k_4} [NX \cdot NN]$$

$$2\,NN \underset{}{\overset{K_3}{\rightleftharpoons}} NN_2$$

$$2\,NX \underset{}{\overset{K_4}{\rightleftharpoons}} NX_2$$

$$NN + NX \underset{}{\overset{K_5}{\rightleftharpoons}} [NN \cdot NX]$$

$$AB + B \xrightarrow{k_1} [B \cdot NN]$$

$$AB + A \xrightarrow{k_1} [A \cdot NN]$$

$$AB + B \xrightarrow{k_1} [B \cdot NX]$$

$$AB + A \xrightarrow{k_1} [A \cdot NX]$$
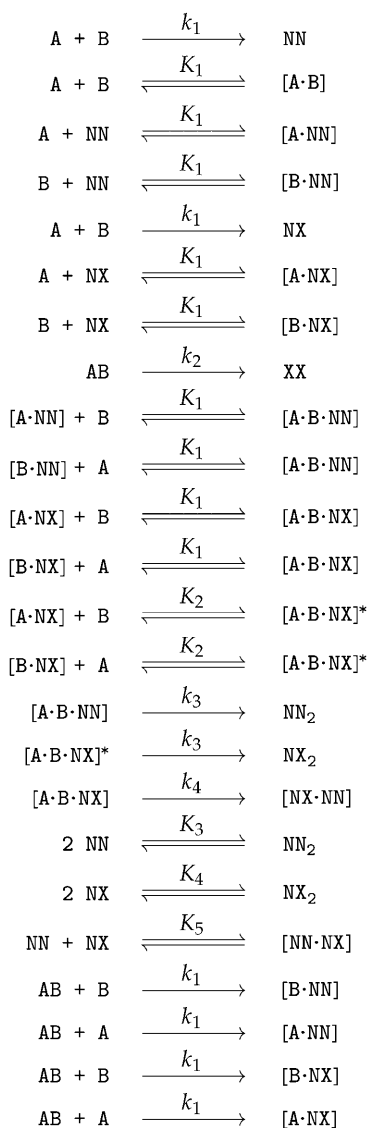
$k_1 = (2.97 \pm 0.02) \times 10^{-4}\,\mathrm{M}^{-1}\mathrm{s}^{-1}$ $K_1 = 1.6 \times 10^2\,\mathrm{M}^{-1}$

$k_2 = (5.21 \pm 0.13) \times 10^{-7}\,\mathrm{s}^{-1}$ $K_2 = 20\,\mathrm{M}^{-1}$

$k_3 = (1.46 \pm 0.00) \times 10^{-2}\,\mathrm{s}^{-1}$ $K_3 = 8.0 \times 10^5\,\mathrm{M}^{-1}$

$k_4 = (8.07 \pm 0.00) \times 10^{-3}\,\mathrm{s}^{-1}$ $K_4 = 8.1 \times 10^3\,\mathrm{M}^{-1}$

$K_5 = 2.5 \times 10^5\,\mathrm{M}^{-1}$

Figure 11. Kinetic model of the system with rate and equilibrium constants. Errors for k_3 and k_4 are smaller than ± 0.005. Such a model is used as an input for Simfit, which will either only simulate concentration–time curves based on given parameters or perform an optimisation of variable parameters to match experimental data.

molecular dynamics simulations of A, B and NN in chloroform was conducted. After equilibrating each system, the diffusion constant—which is proportional to the rate constant in this scenario—was determined from the centre-of-mass mean square displacement by using the Einstein relation. Thus, we arrived at rate constants in the order of $10^{10}\,\mathrm{M}^{-1}\mathrm{s}^{-1}$ for all diffusion-limited processes.

We fitted the variable parameters of our model to experimental data using Simfit.[75] According to the results, the Diels–Alder reaction is efficiently catalysed by templating. The effective kinetic molarity (EM) for autocatalyic pathways is EM $= k_3/k_1 = 50\,\mathrm{M}$ and EM $= k_4/k_1 = 27\,\mathrm{M}$ for cross-catalytic pathways. A reaction to a catalytically inactive XX is very slow compared with all other reaction channels, which is a desirable feature. [A·B·NX]* is destabilised with respect to [A·B·NN] and [A·B·NX] by almost one order of magnitude. Template duplexes also exhibit the same relative stability that was predicted by averaged energies from MD simulations. Having determined the association constants of [A·NN] and [NN·NN], we were able to quantitatively compare them to calculated free energies of dissociation. The kinetic model yields the relationship shown in Equation (3), while we know from our AIMD simulations that the relationship shown in Equation (4) is true. Thus, Equation (2) is fulfilled remarkably well.

$$\frac{\ln K_{[NN \cdot NN]}}{\ln K_{[A \cdot NN]}} \approx 2.67 \tag{3}$$

$$\frac{\Delta G_{\mathrm{diss}}[NN \cdot NN]}{\Delta G_{\mathrm{diss}}[A \cdot NN]} \approx 2.61 \tag{4}$$

Another interesting test for our model would be to probe its ability to correctly predict the effect of initially added product mixture from another reaction. We simulated the effect of adding 10 % product mixture with a composition of NN/NX $= 16$:1 and compared the result to experimental data (Figure 12). The effect on the initial rate of formation of NN is predicted very accurately, while the effect on NX is impossible to measure by NMR spectroscopy. The difference between simulated curves is of the same magnitude as experimental errors arising from integrating small NMR signals. In summary, our model is able to describe the system very well. One has to keep in mind, however, that the number of observables is small relative to the number of variables in the model; this will inevitably cause covariances
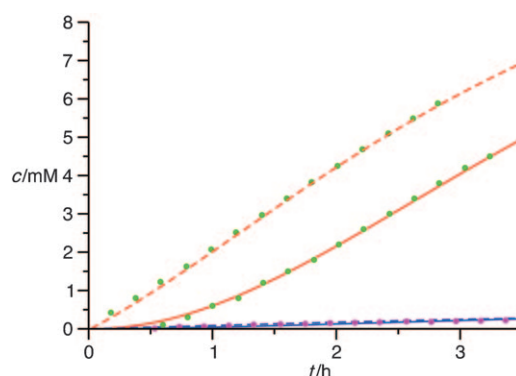
Figure 12. Experimental data and modelling of the effect of initial addition of a 10 % product mixture. ——: NX, model; ——: NN, model; -----: NN, model with the addition of 10 % product; -----: NX, model with the addition of 10 % product; ●: NN, experimental and ●: NX experimental.

between variables, possibly limiting the degree of accuracy with which they can be determined. We have also constructed other kinetic models by changing and reducing the number of parameters directly involved in the auto- and cross-catalytic pathways to probe different mechanisms leading to the observed diastereoselectivity, but they yield less accurate or even unphysical results. The same is true if the assignment of NX and XX is interchanged.

Conclusion

We have presented a new diastereoseletive self-replicating system based on a fulvene Diels–Alder reaction in which two diastereomeric templates compete for common resources. The kinetics of the reaction was measured by time-resolved 1D NMR spectroscopy supported by ab initio chemical shifts. Different diastereomers were identified by ROESY. Whereas in the absence of catalysis there is only a slight diastereoselectivity of 3:2, this changes to 1:16 when replication is enabled. We used AIMD simulations to calculate free-energy profiles and dissociation potentials explaining the observed behaviour: one template acts as a selfish autocatalyst, the other as an altruistic cross-catalyst leading to an intrinsic asymmetry. As a consequence, the autocatalyst dominates the system leading to the observed change in diastereoselectivity. Based on the obtained data, we were able to construct a kinetic model and derive rate and equilibrium constants, which are in agreement with results from our ab initio calculations.

The design of complex chemical reaction networks relies heavily on understanding these systems at a very detailed and fundamental level. However, there will be more and more cases in which the delicate relationship between structure and physicochemical behaviour cannot be analysed by either experiment or theory alone. The field of systems chemistry will have to rely on an intelligent interplay of both; this will lead to a more complete picture of dynamic phenomena in chemistry. We believe that our method of combining 1D and 2D NMR spectroscopic techniques supported by calculated shifts with AIMD simulations is a step in this direction. Although experimental obstacles, namely, the insolubility of products, prevented us from conducting important measurements, we were able to unravel the underlying reaction network and to rationalise the observed change in diastereoselectivity. The two-pronged strategy employed herein has the potential to lead to insights at an unprecedented level not only for other self-replicating systems but for complex chemical networks in general.

Experimental Section

All 1D NMR spectroscopy measurements were carried out on a Bruker DRX 600 spectrometer (600 MHz) at 15 mM concentration of the precursors in $CDCl_3$ (at (293 ± 0.1) K and atmospheric pressure). For kinetic measurements, stock solutions (≈ 30 mM) of each substance were pre-

pared and pipetted into the NMR tube (ratio 1:1) just before starting the measurement. Samples were equilibrated with respect to temperature for 6–8 min inside the spectrometer after mixing, which is sufficient according to information from Bruker. A spectrum with 32 scans was recorded every 10 min. Addition of benzoic acid was done by dissolving the appropriate amount in $CDCl_3$ and using this solution to prepare the stock solutions of both precursors. In case of an initial addition of reaction products, these were taken from an identical and completed reaction, since the products could not be dissolved again after isolation. Adding more than 10% of pre-formed product resulted in precipitation of products at early reaction times. Owing to poor solubility, separation of the isomers by chromatography has not yet been achieved. ROESY spectra were measured in $CDCl_3$ at (293 ± 0.1) K at atmospheric pressure (Bruker DRX 600, TXI-probehead, Topspin 1.3). Parameters were set as follows: 4 K data points per increment (256 increments), 48 scans, 4 dummy scans, 0.1221 s acquisition time, 2.5 s relaxation delay, 5630 Hz spectral width, 200 ms ROESY spin-lock pulse.

The extraction of kinetic data from 1D NMR spectra was performed by using 1D-WINNMR (Bruker Daltonik GmbH, Germany) and custom python scripts to facilitate the manipulation of large data sets. Kinetic simulation and fitting of the data was performed by using Simfit.[75]

Computational Details

General setup of constrained ab initio MD simulations: All calculations were carried out with the CPMD package[76] and set up as follows: The optimised structure was centred in a periodically repeating orthorhombic box of an appropriate size ensuring at least a distance of 3 Å between the molecule and box boundaries. The respective reaction centres were prearranged with a value of $D = 3.6$ Å. The system was equilibrated to an average temperature of 300 K with a standard deviation in the order of 10% by using a Nose–Hoover chain thermostat on the ions.[77,78] The coupled equations of motion for nuclei and molecular orbitals were solved by using the velocity Verlet algorithm with a timestep of 4 a.u. A fictitious mass of 400 a.u was assigned to the electronic degrees of freedom. Core electrons were treated by using Vanderbilt pseudopotentials; valence orbitals were expanded in a plane wave basis with an energy cutoff of 25 Ry. The PBE functional was used for all calculations. For each value of D, the length of production runs was determined by the convergence of the constraint force (typically 2–5 ps). After changing the value of D the system was repeatedly quenched to the Born–Oppenheimer surface. Errors for the free-energy profiles were calculated by measuring the fluctuations of the mean constraint force over the last 0.5 ps. The minimum, maximum and average forces for each value of D were integrated to yield free energies and the respective errors. MEPs were calculated by optimising the geometry of a snapshot randomly taken from the corresponding MD run.

Calculation of thermally averaged shieldings: Thermally averaged, room-temperature magnetic shieldings were calculated for the individual molecules and selected hydrogen-bonded complexes, as well as the $CDCl_3$ solvent, at the B3LYP/6-311G* level by using the Gaussian 03 package[79] by averaging over 20 AIMD snapshots for [NN·NX], 114 snapshots for XX, and 84 snapshots for $CDCl_3$. The snapshots were separated by 1 ps in the case of [NN·NX] and XX, and by 0.5 ps in the case of $CDCl_3$. In analogy to the experimental procedure, the chemical shifts were first calculated with respect to $CDCl_3$. To obtain the final tetramethylsilane (TMS)-based values, a further 7.26 ppm were subtracted. The AIMD simulations were performed by using the same computational parameters as for the constrained AIMD runs detailed in the previous section. The standard deviation in temperature was 25 K and 32 K for [NN·NX] and XX, respectively, and 125 K for $CDCl_3$.

Acknowledgements

[1] M. Kindermann, I. Stahl, M. Reimold, W. M. Pankau, G. von Kiedrowski, *Angew. Chem.* **2005**, *117*, 6908–6913; *Angew. Chem. Int. Ed.* **2005**, *44*, 6750–6755.

[2] J. Stankiewicz, L. Eckardt, *Angew. Chem.* **2006**, *118*, 350–352; *Angew. Chem. Int. Ed.* **2006**, *45*, 342–344.

[3] R. F. Ludlow, S. Otto, *Chem. Soc. Rev.* **2008**, *37*, 101–108.

[4] K. Soai, T. Shibata, H. Morioka, H. Choji, *Nature* **1995**, *378*, 767–768.

[5] T. Shibata, H. Morioka, T. Hayase, K. Choji, K. Soai, *J. Am. Chem. Soc.* **1996**, *118*, 471–472.

[6] T. Kawasaki, Y. Matsumura, T. Tsutsumi, K. Suzuki, M. Ito, K. Soai, *Science* **2009**, *324*, 492–495.

[7] M. Mauksch, S. B. Tsogoeva, I. M. Martynova, S. W. Wei, *Angew. Chem.* **2007**, *119*, 397–400; *Angew. Chem. Int. Ed.* **2007**, *46*, 393–396.

[8] D. G. Blackmond, *Chirality* **2009**, *21*, 359–362.

[9] D. G. Blackmond, M. Klussmann, *Chem. Commun.* **2007**, 3990–3996.

[10] D. G. Blackmond, O. K. Matar, *J. Phys. Chem. B* **2008**, *112*, 5098–5104.

[11] D. G. Blackmond, *Proc. Natl. Acad. Sci. USA* **2004**, *101*, 5732–5736.

[12] D. G. Blackmond, C. R. McMillan, S. Ramdeehul, A. Schorm, J. M. Brown, *J. Am. Chem. Soc.* **2001**, *123*, 10103–10104.

[13] M. Klussmann, H. Iwamura, S. P. Mathew, D. H. Wells Jr. , U. Pandya, A. Armstrong, D. G. Blackmond, *Nature* **2006**, *441*, 621–623.

[14] W. L. Noorduin, T. Izumi, A. Millemaggi, M. Leeman, H. Meekes, W. J. P. Van Enckevort, R. M. Kellogg, B. Kaptein, E. Vlieg, D. G. Blackmond, *J. Am. Chem. Soc.* **2008**, *130*, 1158–1159.

[15] W. L. Noorduin, P. van der Asdonk, H. Meekes, W. J. P. van Enckevort, B. Kaptein, M. Leeman, R. M. Kellogg, E. Vlieg, *Angew. Chem.* **2009**, *121*, 3328–3330; *Angew. Chem. Int. Ed.* **2009**, *48*, 3278–3280.

[16] C. Viedma, J. E. Ortiz, T. de Torres, T. Izumi, D. G. Blackmond, *J. Am. Chem. Soc.* **2008**, *130*, 15274–15275.

[17] T. Buhse, *Tetrahedron: Asymmetry* **2003**, *14*, 1055–1061.

[18] G. Lente, *J. Phys. Chem.* **2005**, *109*, 11058–11063.

[19] T. Satyanarayana, S. Abraham, H. Kagan, *Angew. Chem.* **2009**, *121*, 464–503; *Angew. Chem. Int. Ed.* **2009**, *48*, 456–494.

[20] I. Epstein, J. Pojman, O. Steinbock, *Chaos* **2006**, *16*, 037101–037107.

[21] G. Biosa, S. Bastianoni, M. Rustici, *Chem. Eur. J.* **2006**, *12*, 3430–3437.

[22] G. von Kiedrowski, *Bioorg. Chem. Front.* **1993**, *3*, 113–146.

[23] L. E. Orgel, *Nature* **1992**, *358*, 203–209.

[24] G. von Kiedrowski, *Angew. Chem.* **1986**, *98*, 932–934; *Angew. Chem. Int. Ed. Engl.* **1986**, *25*, 932–935.

[25] G. von Kiedrowski, *40 Jahre Fonds der Chemischen Industrie 1950–1990*, VCI, Frankfurt **1990**, p. 197.

[26] W. S. Zielinski, L. E. Orgel, *Nature* **1987**, *327*, 346–347.

[27] T. Tjivikua, P. Ballester, J. Rebek, *J. Am. Chem. Soc.* **1990**, *112*, 1249–1250.

[28] J. S. Nowick, Q. Feng, T. Tjivikua, P. Ballester, J. Rebek, Jr., *J. Am. Chem. Soc.* **1991**, *113*, 8831–8839.

[29] V. Rotello, J. Hong, J. Rebek, Jr., *J. Am. Chem. Soc.* **1991**, *113*, 9422–9423.

[30] M. Famulok, J. Norwick, J. Rebeck, Jr., *Acta Chem. Scand.* **1992**, *46*, 315–324.

[31] A. Terfort, G. von Kiedrowski, *Angew. Chem.* **1992**, *104*, 626–628; *Angew. Chem. Int. Ed. Engl.* **1992**, *31*, 654–656.

[32] T. Achilles, G. von Kiedrowski, *Angew. Chem.* **1993**, *105*, 1225–1228; *Angew. Chem. Int. Ed. Engl.* **1993**, *32*, 1198–1201.

[33] F. Menger, A. Eliseev, N. A. Khanjin, *J. Am. Chem. Soc.* **1994**, *116*, 3613–3614.

[34] D. Sievers, G. von Kiedrowski, *Nature* **1994**, *369*, 221–224.

[35] E. Wintner, M. Conn, J. Rebek, *J. Am. Chem. Soc.* **1994**, *116*, 8877–8884.

[36] E. Wintner, M. Conn, J. Rebek, Jr., *Acc. Chem. Res.* **1994**, *27*, 198–203.

[37] F. M. Menger, A. V. Eliseev, N. A. Khanjin, M. J. Sherrod, *J. Org. Chem.* **1995**, *60*, 2870–2878.

[38] D. H. Lee, J. R. Granja, J. A. Martinez, K. Severin, M. R. Ghadiri, *Nature* **1996**, *382*, 525–527.

[39] R. Maoz, S. Matlis, E. DiMasro, B. M. Ocko, J. Sagiv, *Nature* **1996**, *384*, 150–153.

[40] D. N. Reinhoudt, D. M. Rudkevich, F. de Jong, *J. Am. Chem. Soc.* **1996**, *118*, 6880–6889.

[41] B. Wang, I. O. Sutherland, *Chem. Commun.* **1997**, 1495–1496.

[42] D. Sievers, G. von Kiedrowski, *Chem. Eur. J.* **1998**, *4*, 629–641.

[43] A. Stauffer, M. Sipper, *Physica D* **1998**, *116*, 71–80.

[44] V. C. Allen, D. Philp, N. Spencer, *Org. Lett.* **2001**, *3*, 777–780.

[45] H. Schöneborn, J. Bülle, G. von Kiedrowski, *ChemBioChem* **2001**, *2*, 922–927.

[46] N. Paul, G. F. Joyce, *Proc. Natl. Acad. Sci. USA* **2002**, *99*, 12733–12740.

[47] E. Kassianidis, R. J. Pearson, D. Philp, *Org. Lett.* **2005**, *7*, 3833–3836.

[48] E. Kassianidis, R. J. Pearson, D. Philp, *Chem. Eur. J.* **2006**, *12*, 8798–8812.

[49] E. Kassianidis, D. Philp, *Angew. Chem.* **2006**, *118*, 6492–6496; *Angew. Chem. Int. Ed.* **2006**, *45*, 6344–6348.

[50] E. Kassianidis, D. Philp, *Chem. Commun.* **2006**, 4072–4074.

[51] E. Kassianidis, R. J. Pearson, E. A. Wood, D. Philp, *Faraday Discuss.* **2010**, *145*, 235–254.

[52] R. J. Pearson, E. Kassianidis, A. M. Z. Slawin, D. Philp, *Chem. Eur. J.* **2006**, *12*, 6829–6840.

[53] V. del Amo, A. M. Z. Slawin, D. Philp, *Org. Lett.* **2008**, *10*, 4589–4592.

[54] J. W. Sadownik, D. Philp, *Angew. Chem.* **2008**, *120*, 10113–10118; *Angew. Chem. Int. Ed.* **2008**, *47*, 9965–9970.

[55] S. Xu, N. Giuseppone, *J. Am. Chem. Soc.* **2008**, *130*, 1826–1827.

[56] B. J. Lam, G. F. Joyce, *Nat. Biotechnol.* **2009**, *27*, 288–292.

[57] T. A. Lincoln, G. F. Joyce, *Science* **2009**, *323*, 1229–1232.

[58] R. Nguyen, L. Allouche, E. Buhler, N. Giuseppone, *Angew. Chem.* **2009**, *121*, 1113–1116; *Angew. Chem. Int. Ed.* **2009**, *48*, 1093–1096.

[59] B. Rubinov, N. Wagner, H. Rapaport, G. Ashkenasy, *Angew. Chem.* **2009**, *121*, 6811–6814; *Angew. Chem. Int. Ed.* **2009**, *48*, 6683–6686.

[60] A. Vidonne, D. Philp, *Eur. J. Org. Chem.* **2009**, 593–610.

[61] A. Vidonne, D. Philp, *Tetrahedron* **2008**, *64*, 8464–8475.

[62] I. Stahl, G. von Kiedrowski, *J. Am. Chem. Soc.* **2006**, *128*, 14014–14015.

[63] N. Wagner, G. Ashkenasy, *Chem. Eur. J.* **2009**, *15*, 1765–1775.

[64] N. Wagner, G. Ashkenasy, *J. Chem. Phys.* **2009**, *130*, 164907/1–6.

[65] P. Walde, R. Wick, M. Fresta, A. Mangone, P. L. Luisi, *J. Am. Chem. Soc.* **1994**, *116*, 11649–11654.

[66] A. Saghatelian, Y. Yokobayashi, K. Soltani, M. R. Ghadiri, *Nature* **2001**, *409*, 797–801.

[67] G. Ashkenasy, M. R. Ghadiri, *J. Am. Chem. Soc.* **2004**, *126*, 11140–11141.

[68] J. R. Nitschke, *Nature* **2009**, *462*, 736–738.

[69] R. Car, M. Parrinello, *Phys. Rev. Lett.* **1985**, *55*, 2471.

[70] V. Allen, C. Robertson, S. Turega, D. Philp, *Org. Lett.* **2010**, *12*, 1920–1923.

[71] N. L. Doltsinis in *NIC Series, Vol. 31* (Eds.: J. Grotendorst, S. Blügel, D. Marx), John von Neumann Institute for Computing, Jülich, **2006**, pp. 375–387.

[72] P. R. L. Markwick, N. L. Doltsinis, J. Schlitter, *J. Chem. Phys.* **2007**, *126*, 045104.

[73] C. Burisch, P. R. L. Markwick, N. L. Doltsinis, J. Schlitter, *J. Chem. Theory Comput.* **2008**, *4*, 164–172.

[74] D. G. Truhlar, *Annu. Rev. Phys. Chem.* **1984**, *35*, 159.

CHEMISTRY
A EUROPEAN JOURNAL

[75] SimFit 32, G. von Kiedrowski, **1990–2010**.

[76] CPMD package, J. Hutter, P. Ballone, M. Bernasconi, P. Focher, E. Fois, S. Goedecker, D. Marx, M. Parrinello, M. Tuckerman, MPI für Festkörperforschung and IBM Zürich Research Laboratory, Stuttgart, **2001**.

[77] S. Nosé, *J. Chem. Phys.* **1984**, *81*, 511.

[78] W. G. Hoover, *Phys. Rev. A* **1985**, *31*, 1695.

[79] Gaussian 03, Revision C.02, M. J. Frisch, G. W. Trucks, H. B. Schlegel, G. E. Scuseria, M. A. Robb, J. R. Cheeseman, J. A. Montgomery, Jr., T. Vreven, K. N. Kudin, J. C. Burant, J. M. Millam, S. S. Iyengar, J. Tomasi, V. Barone, B. Mennucci, M. Cossi, G. Scalmani, N. Rega, G. A. Petersson, H. Nakatsuji, M. Hada, M. Ehara, K. Toyota, R. Fukuda, J. Hasegawa, M. Ishida, T. Nakajima, Y. Honda, O. Kitao, H. Nakai, M. Klene, X. Li, J. E. Knox, H. P. Hratchian, J. B. Cross, V. Bakken, C. Adamo, J. Jaramillo, R. Gomperts, R. E. Stratmann, O. Yazyev, A. J. Austin, R. Cammi, C. Pomelli, J. W. Ochterski, P. Y. Ayala, K. Morokuma, G. A. Voth, P. Salvador, J. J. Dannenberg, V. G. Zakrzewski, S. Dapprich, A. D. Daniels, M. C. Strain, O. Farkas, D. K. Malick, A. D. Rabuck, K. Raghavachari, J. B. Foresman, J. V. Ortiz, Q. Cui, A. G. Baboul, S. Clifford, J. Cioslowski, B. B. Stefanov, G. Liu, A. Liashenko, P. Piskorz, I. Komaromi, R. L. Martin, D. J. Fox, T. Keith, M. A. Al-Laham, C. Y. Peng, A. Nanayakkara, M. Challacombe, P. M. W. Gill, B. Johnson, W. Chen, M. W. Wong, C. Gonzalez, J. A. Pople, Gaussian, Inc., Wallingford CT, **2004**.